A mobile robot with a two-degree-of-freedom suspension for traversing uneven terrain with minimal slip: Modeling, simulation and experiments

Tharakeshwar Appala*, Ashitava Ghosal†

Abstract

It is known in literature that a wheeled mobile robot (WMR) with fixed length axle will slip on an uneven terrain. One way to avoid wheel slip is to use a torus-shaped wheel with lateral tilt capability which allows the distance between the wheel-ground contact points to change even with a fixed length axle. Such an arrangement needs a two degree-of-freedom (DOF) suspension for the vertical and lateral tilting motion of the wheel. In this paper modeling, simulation, design and experimentation with a three-wheeled mobile robot, with torus-shaped wheels and a novel two DOF suspension allowing independent lateral tilt and vertical motion, is presented. The suspension is based on a four-bar mechanism and is called the double four-bar (D4Bar) suspension. Numerical simulations show that the three-wheeled mobile robot can traverse uneven terrain with low wheel slip. Experiments with a prototype three-wheeled mobile robot moving on a constructed uneven terrain along a straight line, a circular arc and a path representing a lane change, also illustrate the low slip capability of the three-wheeled mobile robot with the D4Bar suspension.

Keyword: Uneven terrain, Wheel slip, Lateral tilt, Torus-shaped wheels, Two-degree-of-freedom suspension, Wheeled mobile robot.

1 Introduction

An increasingly important new application of mobile robots is motion and navigation on uneven and rough terrains. Wheels in a wheeled mobile robot, moving on a plane surface, are often assumed to be undergoing pure rolling or slip-free motion. In general, two wheels joined by a common rigid axle cannot roll on an uneven terrain without slip since there is no instantaneous centre compatible with both the wheels [1]. Slip at the wheel-ground contact points leads to localization errors when

*Associate Professor in Mechanical Engineering Department, SSJ Engineering College, Hyderabad 500075, India. Email: tharakcontact@gmail.com, Tel. +91 8413-234289

†Professor, Department of Mechanical Engineering, Indian Institute of Science, Bangalore 560012, India. Corresponding author. E-mail: asitava@mecheng.iisc.ernet.in, Tel. +91 80 2293 2956

only on-board odometer is used and wastes power which is often at a premium in activities such as planetary exploration. To overcome wheel slip, the distance between the wheel-ground contact points needs to change so that a common instantaneous centre exists. Researchers have proposed two approaches to avoid kinematic wheel slip – the variable axle length approach [2] allows the axle length to vary when the mobile robot moves on the uneven terrain and the wheel lateral tilt approach allows the wheel to tilt laterally while moving on the uneven terrain thereby effectively changing the wheel-ground contact distance without changing the axle length [3, 4]. The lateral tilt changes the wheel camber angle and this has been termed as passive variable camber (PVC) [5]. However, in all the above mentioned works, experimental evidence is not presented. In this paper, we explore the wheel lateral tilt approach and provide numerical simulation and experimental results for a three-wheeled mobile robot traversing an uneven terrain.

For wheel lateral tilt on uneven terrain, a two degree-of-freedom (DOF) suspension is required – one to accommodate the vertical motion of the wheel and a second to allow lateral tilting. There exists various suspension mechanism, developed by NASA and others (see, for example, [6, 7, 8, 9, 10, 11]) for traversing uneven terrain in planetary exploration and moving over rough terrain. All the suspension are for vehicles with several wheels – six wheels in Rover, Spirit and Opportunity, five wheels in Micro5 and four in the vehicle described in reference [10]. Moreover, the main goal of the developed suspensions is to navigate the rough and uneven terrain, maintain wheel-terrain contact in a stable manner and go over "small" obstacles and ditches. Avoiding or minimizing wheel slip is not the primary concern in these applications. In this paper, we present a three-wheeled mobile robot, with torus-shaped wheels and a novel two DOF suspension, capable of moving on uneven terrains with low slip.

Existing one DOF suspension systems accommodate the wheel vertical travel and ensure that the wheel-ground contact is maintained. Camber angle, equivalent to lateral tilt, provided in existing one-DOF suspension is fixed. Most one DOF suspension mechanisms presented in vehicle technology textbooks (see for example, Brandy [12] and Dixon [13]) use simple leaf springs for heavy

duty vehicles and arrangements such as double wishbone, Macpherson suspension with springs, dampers and mechanism combinations for passenger cars. These suspension mechanisms do not allow lateral tilt required at the wheels. Sebe [14] and more recently Krajekian [15] present a suspension system for vehicles where variable camber can be obtained. In their design, camber control rods are united at the centre of the vehicle on a plate which is articulated to the chassis and the embodiment formulates an approximate parallelogram linkage which can change the camber of both the wheels by an equal amount. Other researchers [16, 17, 18] have patented variable camber suspensions for vehicles by detecting the lateral force acting on the vehicle in turning. In these patents, a negative camber is set for the outer wheel and a positive camber is set for the inner wheel based on the measured force. In all the above mentioned patents and designs, the resulting camber angles for both the wheels, connected by the axle, are dependent making the mechanisms unsuitable for independent lateral tilting of the wheels. For a wheel with independent lateral tilt capability, a two DOF suspension mechanism is required – one for maintaining wheel contact with terrain in the vertical direction and other for the lateral tilting of the wheel. Tharakeshwar [19] proposed six possible two DOF suspension mechanisms and presented simulations of a three-wheeled mobile robot, with torus-shaped wheels equipped with the two DOF suspensions, traversing uneven terrains. In a recent publication [20], simulation and experimental results with a modified common trailing arm suspension mechanism is presented. In this work a significantly better and novel suspension system, in terms of decreased wheel slip and ease of manufacturability, named as the double four-bar (D4Bar) suspension mechanism is presented. This paper deals with modeling, simulation and experiments with a three-wheeled mobile robot equipped with two DOF D4Bar suspension mechanisms and moving on uneven terrain. Three representative paths, namely a straight line, a circular arc and a path representing a lane change are used for simulation and experiments. It is shown that the three-wheeled mobile robot can traverse uneven terrain with low slip and, furthermore, if the suspension is not used and the lateral tilting is not allowed, the slip is significantly larger. The simulation and experimental results presented in this paper proves the

feasibility of reducing slip in WMR by using the wheel lateral tilt concept.

The paper is organized as follows: In section 2, for the sake of completeness, the modeling a torus-shaped wheel moving on an uneven terrain and a three-wheeled mobile robot equipped with three torus-shaped wheels are presented. Section 2 also describes the two DOF D4Bar suspension used to enable lateral tilting of the torus-shaped wheel. In section 3 the details of the uneven terrain and parameter values used in the numerical simulations are presented. Section 3 also presents numerical simulation results for three representative trajectories, with and without suspension. Section 4 deals with the design and prototyping of the D4Bar suspension mechanism and fabrication of WMR with the D4Bar suspension. The prototype wheeled mobile robot with the D4Bar suspension was made to traverse on uneven terrains and the results and discussion on the experimentation are presented in section 4. Finally, the conclusions are presented in section 5.

2 Modeling of WMR and D4Bar suspension

In this section, we first present in brief the equations governing the motion of a torus-shaped wheel moving on a uneven terrain and modeling of a three-wheeled mobile robot equipped with the torus-shaped wheels (see reference [3, 4] for details). Next we present the details of the D4Bar mechanism and simulation of the WMR robot on uneven terrain with and without the D4Bar suspension mechanism. Three simulations, namely a straight line, a circular arc and a path representing a lane change are studied. Results of the simulations show that the slip can be significantly minimized when the suspension mechanism is used.

2.1 Torus-shaped wheel and three-wheeled mobile robot

Figure 1 shows the schematic of a torus-shaped wheel in contact with an uneven surface. The parametric equation of a torus-shaped wheel is given by

$$\mathbf{X}(u,v) = (x,y,z)^{\mathrm{T}} = \begin{pmatrix} r_1\cos(u) \\ \cos(v)(r_2 + r_1\sin(u)) \\ \sin(v)(r_2 + r_1\sin(u)) \end{pmatrix} \tag{1}$$

where (x, y, z) are the coordinates of an arbitrary point on the torus-shaped wheel with respect to a coordinate system $\{W\}$ at the centre of the torus-shaped wheel, r_1 and r_2 are the two radii associated with the torus and (u, v) are the two independent parameters in the vector function $\mathbf{X}(u, v)$ representing the equation of the torus surface. The axis X_w and Y_w are in the central plane of the torus and Z_w is normal to this plane as shown schematically in figure 1. As mentioned later in section 3, the uneven surface is generated from a constructed uneven terrain by taking a large number of points and using smooth interpolation.

Following the development in reference [3], we assign two auxiliary coordinate systems $\{1\}$ and $\{2\}$ at the point of contact, ${}^0\mathbf{p}$, of the torus-shaped wheel and the uneven surface. Denoting the equations of the uneven surface by $\mathbf{X}(u_1, v_1)$, the coordinate axis $\mathbf{X}_1$ is chosen along the vector $\dfrac{\partial \mathbf{X}(u_1, v_1)}{\partial u_1}$, the coordinate axis $\mathbf{Z}_1$ is chosen along the normal given by the cross-product $\dfrac{\partial \mathbf{X}(u_1, v_1)}{\partial u_1} \times \dfrac{\partial \mathbf{X}(u_1, v_1)}{\partial v_1}$ and the $\mathbf{Y}_1$ axis is obtained from the right-hand rule. Similar for the torus surface given by $\mathbf{X}(u_2, v_2)$, the coordinate axis $\mathbf{X}_2$ is along the partial derivative of $\mathbf{X}(u_2, v_2)$ with respect to u_2, $\mathbf{Z}_2$ is along the normal vector to the torus surface. The angle between $\mathbf{X}_1$ and $\mathbf{X}_2$ is denoted by Ψ. Figure 1 shows the relevant coordinate axes and the angle Ψ.

The five independent parameters, (u_1, v_1), (u_2, v_2) and the angle Ψ at ${}^0\mathbf{p}$, completely describe the contact between the torus-shaped wheel and the uneven terrain. As presented first by Montana [21], the time evolution of the five independent variables can be written as

$$\begin{aligned}
(\dot{u}_1, \dot{v}_1)^T &= [M_1]^{-1}([K_1] + [K*])^{-1} \left[(-\omega_y, \omega_x)^T - [K*](V_x, V_y)^T\right] \\
(\dot{u}_2, \dot{v}_2)^T &= [M_2]^{-1}[R_\Psi]([K_1] + [K*])^{-1} \left[(-\omega_y, \omega_x)^T - [K_1](V_x, V_y)^T\right] \\
\dot{\Psi} &= \omega_z + [T_1][M_1](\dot{u}_1, \dot{v}_1)^T + [T_2][M_2](\dot{u}_2, \dot{v}_2)^T \\
0 &= V_z
\end{aligned} \tag{2}$$

where $\dot{u}_i, \dot{v}_i,\ (i = 1, 2)$ are the rate of change of independent parameters describing the uneven surface and the torus-shaped wheel, ω_x, ω_y and ω_z are the angular velocity components, V_x, V_y and V_z are the linear velocity components of the torus-shaped wheel with respect to the uneven terrain,

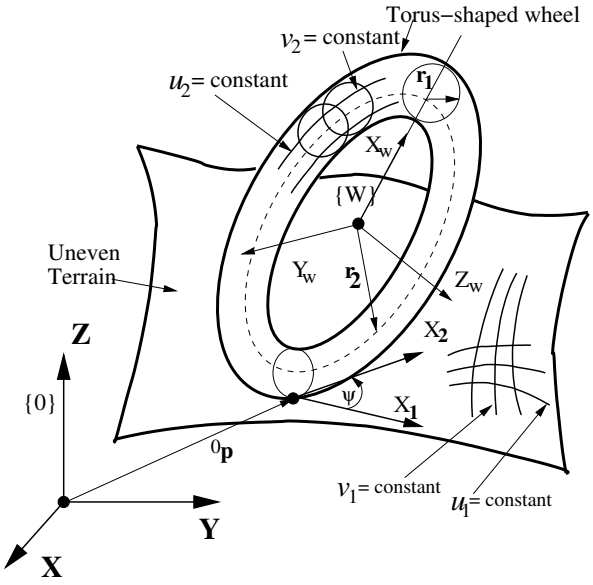

Figure 1: Torus-shaped wheel on uneven terrain

the matrices $[M_1]$, $[M_2]$, $[K_1]$, $[K_2]$, $[K*]$, $[T_1]$, $[T_2]$ are determined from the first and second partial derivatives of the vector functions $\mathbf{X}(u_1, v_1)$ and $\mathbf{X}(u_2, v_2)$ representing the surface torus-shaped wheel and uneven surface at the point of contact and $[R_\Psi]$ is a rotation matrix (refer to [3] for details). It may be noted that $V_z = 0$ since the wheel cannot lose contact with terrain surface. Pure rolling and no slip occurs when $V_x = V_y = 0$. If $\omega_x = \omega_y = 0$, then the surfaces are in pure sliding. In our case, we are interested in pure rolling without slip.

The five ordinary differential equations (ODEs) in five variables given in equation (2) describe the wheel-terrain contact and for pure rolling without slip there are two velocity or *non-holonomic* constraints. The non-holonomic constraints restrict the space of velocities and hence the three degrees of freedom are *instantaneous*. It maybe noted that the wheel-terrain contact is very different from a typical spherical joint which also has three degrees of freedom. In this work, the uneven terrain is assumed to be smooth and hard and the equations of the surface representing the uneven terrain are assumed to be sufficiently differentiable such that matrices $[M_1]$, $[M_2]$, $[K_1]$, $[K_2]$, $[K*]$, $[T_1]$, $[T_2]$ exists and are continuous and differentiable. Uneven terrains with loose soil, dirt, water etc. are not considered in this work.

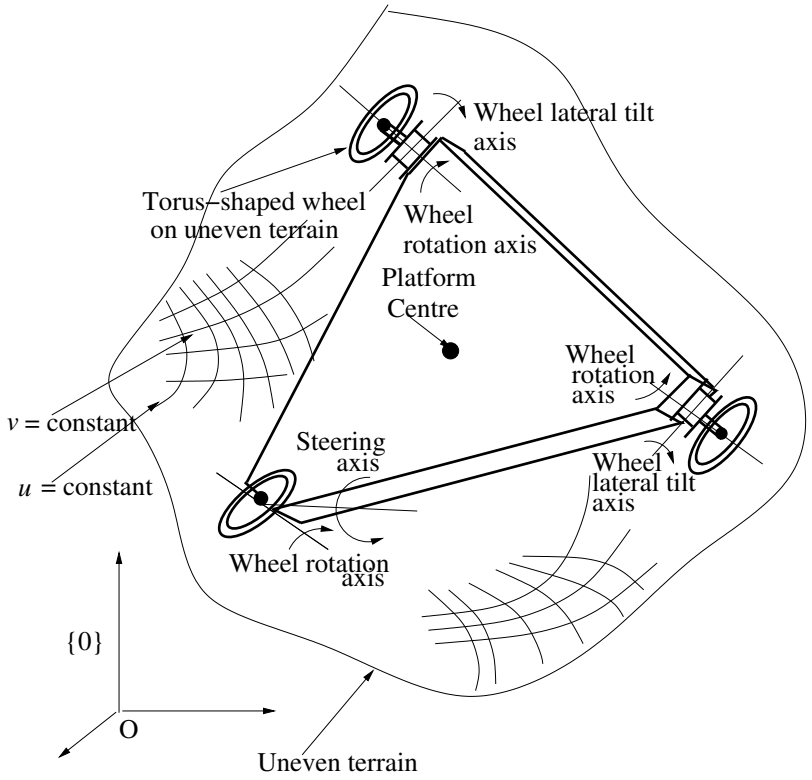

Figure 2: A three-wheeled mobile robot with torus-shaped wheels on uneven terrain

Figure 2 shows a schematic of a three-wheeled mobile robot with the torus-shaped wheels. The two rear wheels can tilt laterally and rotate about their wheel rotation axis while the front wheel can be steered and can also rotate about the wheel rotation axis. As shown in reference [3, 4], the three-wheeled mobile robot on an uneven terrain can be modeled *instantaneously* as hybrid parallel manipulator. Using the well-known Grublër-Kutzbach criterion

$$dof = 6(n - j - 1) + \sum_{i=1}^{n} f_i$$

with total number of links n as 8, the total number of joints j as 9 and total number of degree of freedom, $\sum_{i=1}^{n} f_i$ as 15 (3 for each wheel ground contact point, 3 for the rotation of the wheels about their axis, 2 for the lateral tilting of the rear wheels and 1 for steering of the front wheel), the degree of freedom, dof, of equivalent hybrid-parallel manipulator is obtained as 3. It may be noted that the dof is instantaneous since the three degree of freedom at the wheel-terrain contact

is instantaneous.

The WMR with three degrees of freedom require three independent inputs to traverse an arbitrary uneven terrain. The three natural inputs are the angular speeds of the two rear wheels and steering at the front wheel. The lateral tilting of the rear wheels and the rotation of the front wheel about its axis are passive and can be determined once the three inputs are known. It may be noted that the direct and inverse kinematics (given the three inputs obtain the position and orientation of the WMR platform and vice-versa) of the three-wheeled mobile robot on uneven terrain requires the solution of a system of differential-algebraic equations (DAEs) (see [3] for details).

Using the kinematics equations, the kinetic and potential energy of each of the torus-shaped wheels, the platform and the links representing the passive degrees of freedom can be obtained. Using the Lagrangian formulation, the dynamic equations of motion of the three-wheeled mobile platform can then be obtained. As shown in Chakraborty and Ghosal [4], the dynamic equations of motion are a set of 27 second-order ODEs. Since there are 21 ODEs (describing the kinematics) and three holonomic constraints (describing constant distance between three wheel centres), there can be three independent torque inputs. The three independent inputs are again about the rotation axis of the two rear wheels and the front steering input. The set of DAEs can be solved numerically to simulate the motion of the three-wheeled mobile robot on uneven terrains and as shown [4], the three-wheeled mobile robot can negotiate uneven terrains without slip. In Chakraborty and Ghosal [4], the dynamic equations of motion obtained in closed-form and solved numerically using the commercial software Matlab [22]. In this work, we have used ADAMS [23] for modeling and simulation instead of deriving and numerical solving the DAEs. The main reasons are a) ease of modeling of all the components, including the two-DOF suspension, of the three-wheeled mobile robot in a CAD software, b) ease of importing the complete model of the three-wheeled mobile robot in ADAMS/View and ease of assigning mass and inertial properties to each of the components of the model, and finally c) ease of simulation using the various readily available integration routines, such as GSTIFF, in ADAMS/Solver. There is no need to formulate the DAEs and the software

allows the user to provide arbitrary inputs, initial conditions etc. once a model is created.

The ADAMS software allows imposition of 3D solid to solid contact constraint between two surfaces with an option for applying a frictional force at the contact point. It uses iterative refinement to ensure that penetration between the two contacting geometries is minimal at the contact point. We model the wheel-terrain contact using *contact* tool of ADAMS. The penetration is set at 0.001 mm and following the well-known automotive handbook [24], the static and dynamic resistance at wheel-terrain contact is chosen as 0.9 and 0.8, respectively

As the three-wheeled mobile robot moves on the uneven terrain, the two rear torus-shaped wheels tilts laterally as well they move up and down on the uneven terrain. This implies that the rear wheels of the WMR must have a two DOF suspension which can accommodate vertical motion as well as lateral tilting – the front wheel does not tilt laterally and hence does not require a two DOF suspension. In Chakraborty and Ghosal [4], a simple spring is used to limit the lateral tilting. In Tharakeshwar [19], 6 possible two DOF suspensions are proposed and extensive simulations show that a two DOF suspension based on a double four-bar mechanism, called as the D4bar suspension, performs the best in terms of wheel slip and path deviation from a desired trajectory. This two DOF suspension is described next. In later sections, we show simulation and experimental results for a three-wheeled mobile robot, equipped with the D4Bar suspension, moving on an uneven terrain.

2.2 Two DOF suspension mechanism

Figure 3 shows the schematic of a two DOF suspension which connects the torus-shaped wheel to the WMR platform. The suspension mechanism consists of Mount, a 4-bar mechanism made by four links, L1, L2, L3 and L4 and Wheel hub. The Mount, in the shape of a bracket, is fixed to WMR platform. It holds L1 through a revolute joint at the centre of the link and L1 is free to rotate by an angle on either side about its centre. The links L2 and L3 are connected to L1 and L4 and forms a 4 bar mechanism with L4 fixed with the wheel hub. The torus-shaped wheel is free to rotate about the wheel hub. In this mechanism three springs, S1, S2 and S3 are used. The number of links used in the mechanism are five (platform or Mount, four links L1, L2, L3 and L4) connected

with five revolute joints. The degree of freedom of the mechanism using Grübler's criterion is two. The arrangement of links, joints and springs allows the wheel to travel in the vertical direction and tilt laterally. Figure 3 show schematically the two DOF D4Bar suspension mechanism.

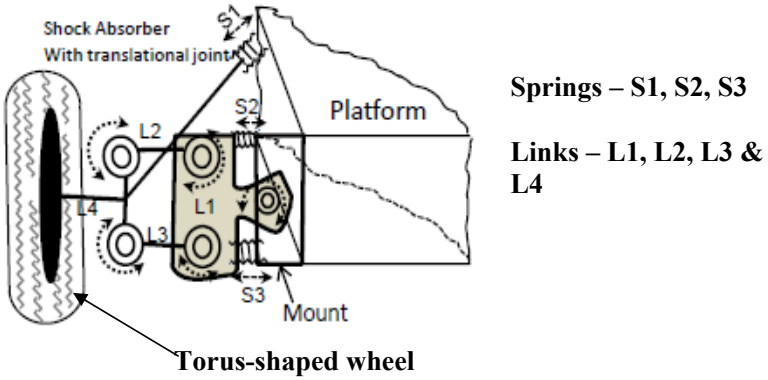

Figure 3: The two DOF D4Bar suspension

3 Modeling and numerical simulation

The use of computer aided kinematic and dynamic simulation has emerged as powerful tool for the modeling and analysis in robotics. We use the commercial software ADAMS/View [23] for modeling the three-wheeled mobile robot with the D4Bar suspension. The lateral tilt in the two rear wheels are restricted to 30° on either side. The platform has a triangular shape with mass of approximately 1.0 kg. The two radii of the torus-shaped wheel are 45 and 15 mm, respectively. The wheel assembly weighs 0.1 kg and the mass of suspension mechanism is 0.2 kg. The aggregate weight of the WMR is made same as that of the constructed prototype (see section 4) with a value of 1.65 kg. The mass inertia tensor components[1] are $I_{xx} = 2.912E + 4$ kg-mm^2, $I_{yy} = 6.19E + 4$ kg-mm^2, $I_{zz} = 3.66E + 4$ kg-mm^2, $I_{xy} = -119.76$ kg-mm^2, $I_{zx} = -316.41$ kg-mm^2, $I_{yz} = -20.146$ kg-mm^2 and the three wheel-ground contacts, in the untilted state of the wheels, form an equilateral triangle of side 30 cm. The stiffness, damping and pre-load of spring S1 (used to accommodate vertical motion) is chosen as 20.0 N-mm^{-1}, 0.65 N-s-mm^{-1} and 25 N, respectively and these are

[1]The numerical values of mass, inertia etc. are obtained from the CAD model created in ADAMS/View.

close to the values of the spring S1 used in the developed hardware. Two similar springs, S2 and S3 with spring stiffness of 5.0 N-mm^{-1}, damping coefficient of 0.65 N-s-mm^{-1} and a pre-load of 10.0 N are connected between two ends of L1 and two slots provided in the Mount.

Several uneven surface were constructed [19] for simulation and experiments and here we present representative results for an uneven terrain which has small slopes and smooth peaks (see experimental results and photograph of the uneven surface in section 4). The maximum slope/grade is about in 1 in 4 and the maximum height of the peak is 50 mm – this is about 1.1 times the major radius and 3.3 times the minor radius of the torus-shaped wheels used in the three-wheeled mobile robot. At a large number of surface points, the elevation (height) was measured and these data points were used to generate the uneven surface using a commercial software SolidWorks [25]. The generated torus-shaped surface (from equation (1)) and the uneven terrain are imported into ADAMS/View for the numerical simulations.

Two types of simulations, namely a) obtain the motion of the centre of mass of the platform for given rotational inputs to the rear wheel and steering input to the front wheel and b) obtain the rotation of the rear wheels and the steering of the front wheel for a desired path of the centre of mass of the platform, were preformed. To test the effectiveness of the two DOF suspension, simulations were performed with the two DOF suspension and without the two DOF suspension, i.e., the wheels were not allowed to tilt laterally. Three sets of simulation results, namely for a straight line path, a circular arc and a path representing a lane change, are presented and discussed next.

Straight line motion

For the straight line motion, the WMR centre is made to move on a straight line at 2 m/sec. The magnitude of the slip velocity[2], $\sqrt{V_x^2 + V_z^2}$, is estimated at wheel-terrain contact point as function of time for the left and right rear wheels. The simulation results are presented in figure 4(a) and

[2]Due to the axis convention in ADAMS, the elevation of the uneven terrain is along the Y axis and the (U_2, V_2) coordinates for the surface are X and Z, respectively. This is different from the notation used in equations (1) and (2).

(b) and it shows that D4Bar leads to a 30 to 40% reduction in slip as compared to the case when the D4Bar suspension is not used. Due to the reduction in slip, the path traced by the WMR centre of mass will deviate less from the desired straight line path. The paths followed by wheeled mobile robot centre of mass for straight line motion is shown in figures 4(c). From the simulation, the maximum path deviation with and without suspension is found to be 11.34 mm and 26.68 mm, respectively. It can be clearly seen that the performance in terms of wheel slip and path deviation is significantly better with the D4Bar suspension and when the wheel lateral tilting is allowed.

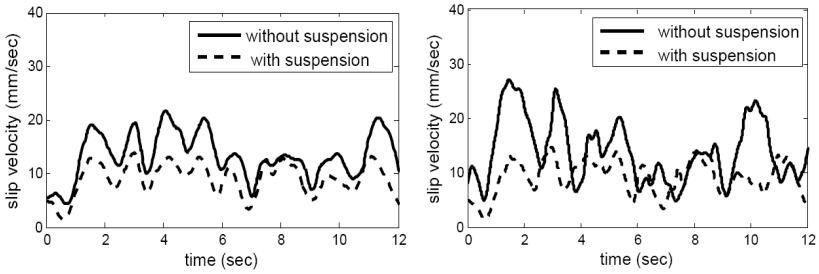

(a) Slip velocity at left wheel

(b) Slip velocity at right wheel

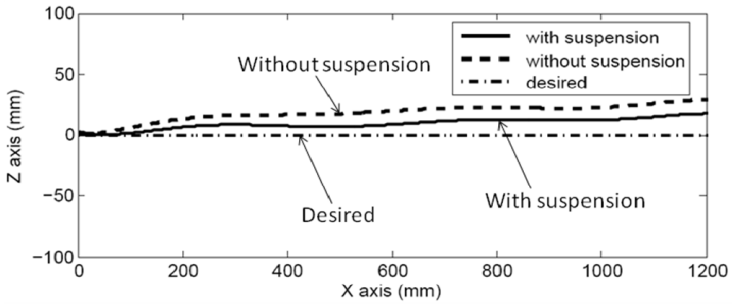

(c) Straight line path with and without suspension

Figure 4: Numerical simulation of straight line motion

Circular motion

For the circular motion, in addition to the inputs to the rear wheels, a constant 30° steering input is given to the front wheel and simulation are conducted with and without the D4Bar suspension mechanism. The slip velocity of the left and right wheel are shown in figure 5(a) and (b). As can be seen, the WMR equipped with D4Bar suspension leads to a 55 to 68% reduction in slip at the wheel-terrain contact point. Figure 6(a) shows the path traced by the WMR and figure 6(b)

shows the error from the desired path with and without suspension. From the simulation, the maximum path deviation from the desired path is obtained as 12.3 mm and 28.2 mm, with and without suspension, respectively. It can be seen, that the performance in terms of wheel slip and path deviation is significantly improved with the D4Bar suspension.

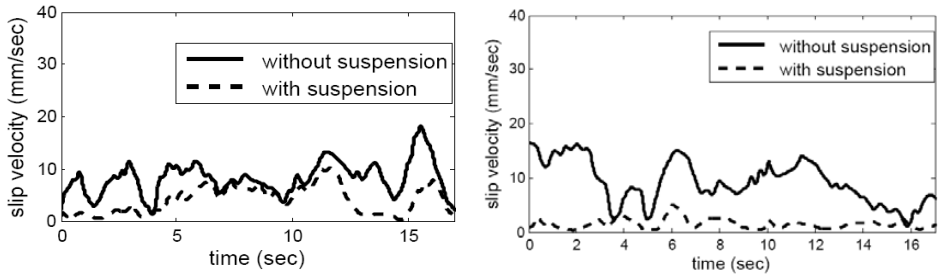

(a) Left wheel slip velocity (b) Right wheel slip velocity

Figure 5: Wheel slip in circular motion

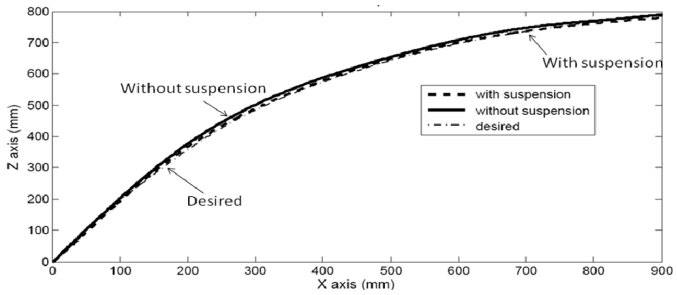

(a) Circular path with and without suspension

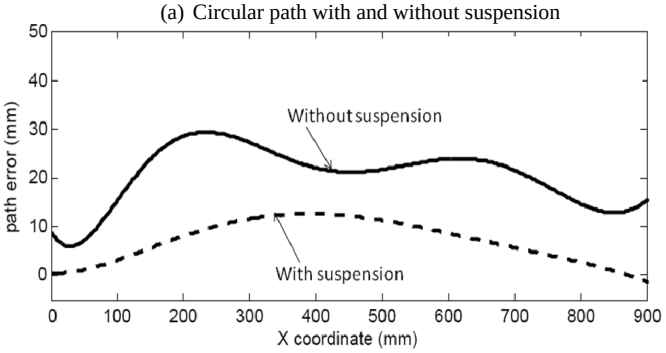

(b) Error between desired and simulated path

Figure 6: Simulation of circular motion and error from desired path

A lane change motion

In the lane change motion, unlike zero steering input in straight line motion and fixed steering input in the circular motion, the steering input continuously changes to navigate in a lane change path. In figure 7(a) and (b), the solid line represents the slip at the wheel-ground contact, for the left and right rear wheel, without the D4Bar suspension and dotted line represents wheel slip with the suspension. One can observe that there is almost 70 to 80% reduction in wheel slip when the suspension is used and wheel lateral tilt is allowed. In the lane change simulation, the maximum deviation was obtained as 5.9 mm and 23.57 mm, with and without suspension, respectively.

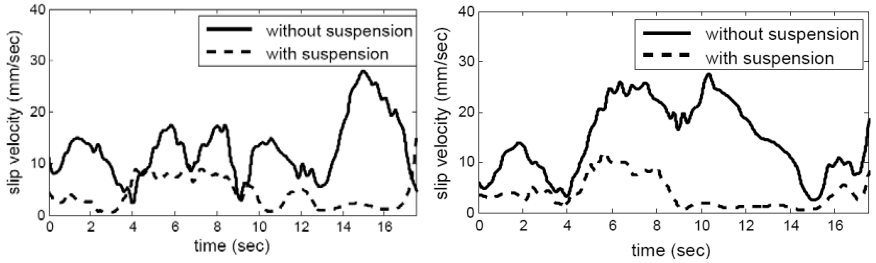

(a) Left wheel slip velocity

(b) Right wheel slip velocity

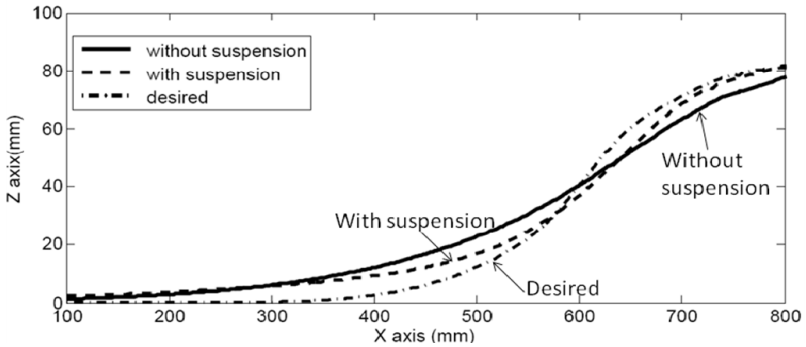

(c) Lane change path with and without suspension

Figure 7: Simulation of a lane change motion

From the three simulation results presented above, we can conclude that the proposed D4Bar suspension is effective in reducing wheel slip and path deviation. It also validates the notion that passive lateral tilting of the torus-shaped wheels in the WMR will lead to significantly less wheel slip when the WMR traverses an uneven terrain. In the next section, we present experimental evidence.

4 Design, fabrication and experiments

As mentioned earlier the rear torus-shaped wheels must be allowed to tilt laterally with respect to centre of the wheel. In our design the D4Bar suspension mechanism is fixed close to the centre of the torus-shaped wheel but, due to the difficulty of placing two joints at the same place, the tilting axis does not pass through the centre of the wheel. The other key elements of the design of torus-shaped wheel and the three-wheeled mobile robot are as follows:

- The torus-shaped wheels should have a reasonably high coefficient of friction so that enough traction is generated between the wheel and ground. This was achieved by using a rubber coating on the wheel and use of cement plaster for the uneven terrain.

- Ideally (also assumed in simulations) there should be point contact between the wheel and uneven terrain. The torus-shaped wheel should deform as little as possible so that the approximation of point contact between wheel and terrain can be used. Although exact point contact was not possible the combination of rubber coated plastic wheel and cement plaster resulted in very little deformation.

- The design of the links and springs in the D4Bar suspension is such that the lateral tilt angle of $\pm 30^\circ$ is obtained. To perform experiments without lateral tilting, a simple lateral tilt locking mechanism was included for the rear wheels.

- Torque transmission from motors to wheels should be possible at all lateral tilts of the rear driving wheels. Three on-board motors are used to actuate the rear wheels and steering of the front wheel. All the motors need to be fixed on the platform and controller and energy source for the motors are also mounted on the platform. We have used motors, controllers and power source from a readily available LEGO Mindstorm NXT kit [26]. One of the advantage of using the LEGO power source and controller is the ease of programming and control of the three motors used in the prototype.

- The weight of the platform was about 1.0 kg and the full prototype was approximately 1.65 kg.

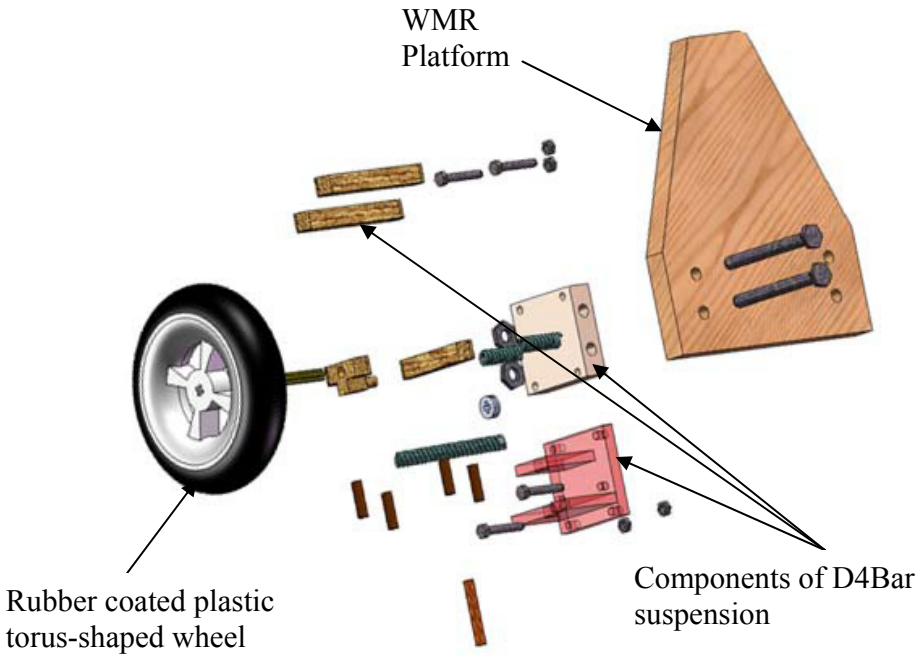

Figure 8: Exploded view of one wheel, suspension components and WMR platform

Figure 8 shows the components of the D4Bar suspension which connects the torus-shaped wheel to the WMR platform.

A key part of the suspension are the three springs helical compression S1, S2 and S3. The spring S1 was designed such that the torus-shaped wheel could go over the bumps on the surface and the springs S2 and S3 were designed such that the WMR could resist its self weight and also allowed $\pm 30^\circ$ lateral tilt in the rear wheels. The springs material was chosen as 414 stainless steel with a G value of approx 77.2 GPa. The number of turns, N, wire diameter d and coil diameter D and other parameters of the springs were designed after trial and error and experimentation. The following values were finally chosen for the springs:

- For spring S1: $d = 1.2$ mm, $D = 4.0$ mm, $N = 15$ and the spring stiffness K is computed to be 20.84 N/mm.

- For spring S2 and S3: $d = 1.2$ mm, $D = 7.0$ mm, $N = 12$ and the spring stiffness K is found to be 4.86 N/mm.

It may be noted that the stiffness of the springs S1 and S2, S3 used in the numerical simulations were 20 N/mm and 5 N/mm, respectively. The values are close to springs used in WMR prototype.

One of the key challenges in building the WMR was to transmit power from the motors to the torus-shaped wheels, with lateral tilting and vertical motion, traversing the uneven terrain. Several concepts such as using flexible cables were attempted. Finally we narrowed down to the use of bevel gears and two DOF Hooke or universal joints. The use of Hooke joints allowed motion transmission even when the wheels were tilted or moving vertically. The transmission arrangement is shown schematically in figure 9.

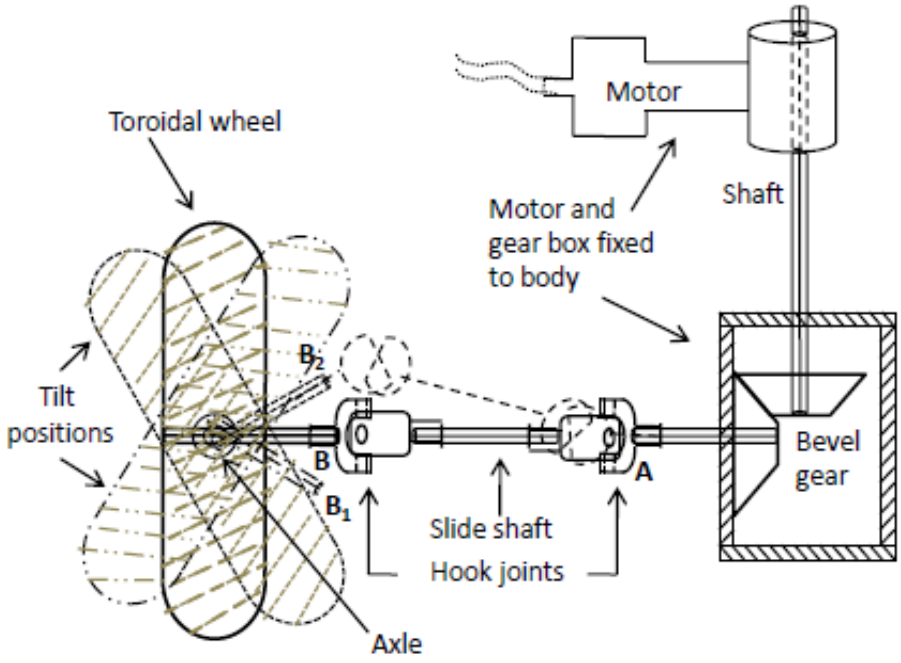

Figure 9: Schematic of arrangement for transmission of power

On the platform a small hole at the centre of mass was drilled to insert a marker for tracing the path traced by the WMR on the uneven terrain.

4.1 Experiments and discussions

The top view of the WMR prototype is shown in figure 10 which also shows the two extreme wheel lateral positions on a flat ground. With the available hardware, it was not possible to measure slip at the wheel-ground contact point. We could however easily trace the path of the platform centre and obtain the error from the desired path as well as compare with the simulation results. These are presented for each of the three paths next.

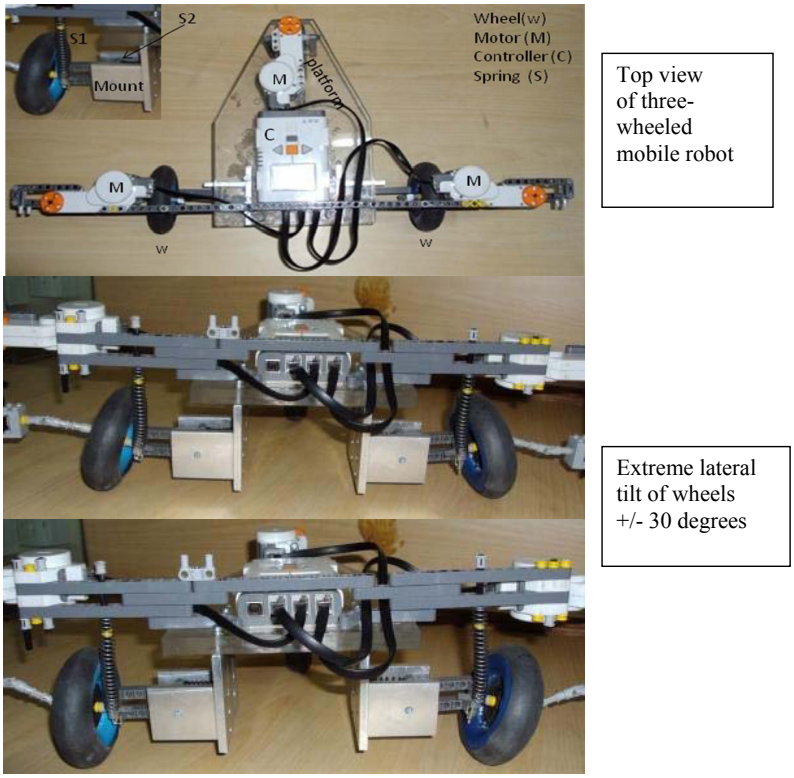

Figure 10: Prototype three-wheeled WMR

Straight line motion

For the straight line path equal inputs are given to the two rear wheels and zero input to the front steering wheel. Several experiments were done and figure 11 shows snapshots of one such trial and the path traced by the marker placed at the centre of the platform. Figure 12 shows the path traced by the marker placed at the platform centre along two diagonals of the uneven terrain surface –

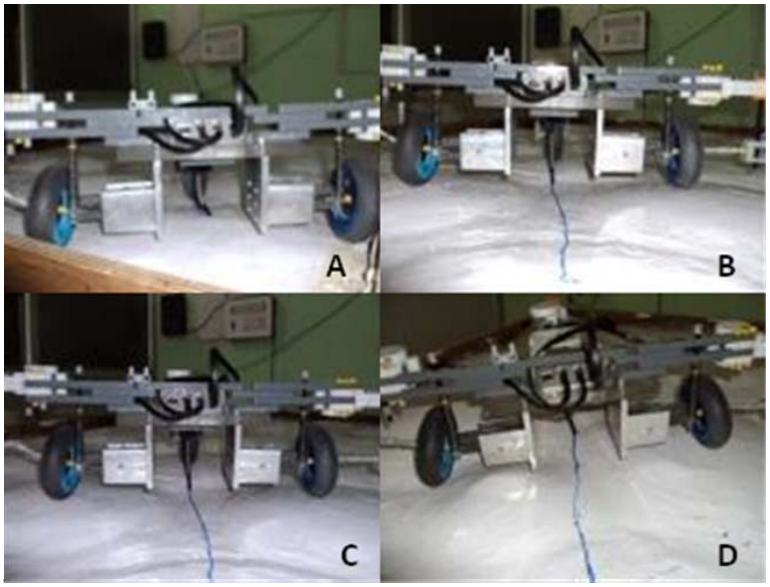

Figure 11: Snapshots of straight line motion of the WMR

the bumps and valleys on the uneven terrain are also visible in the photograph. The trace in red color is when the D4Bar suspension is not used and lateral tilting of the wheels is not allowed. The trace in blue color is when the D4Bar suspension is used and thus lateral tilting of the rear wheels are allowed. Figure 13(a) shows the plots of the paths traced by the WMR with and without

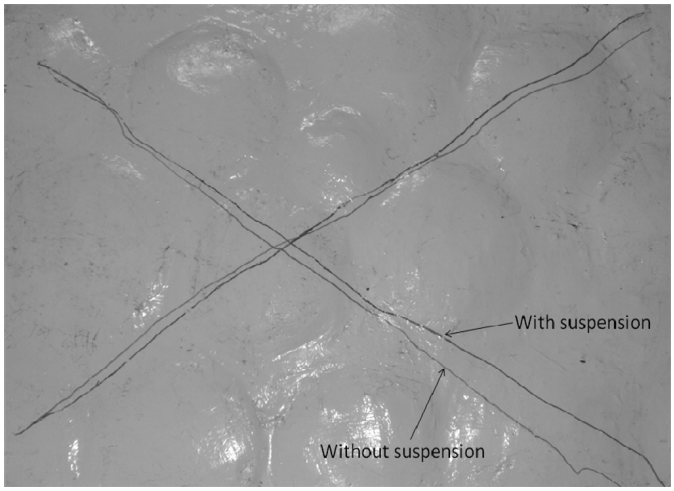

Figure 12: Straight line path with and without suspension

suspension. Figure 13(a) also shows the desired straight line path and the results obtained from

numerical simulations. It maybe noted that the axis of the experimental plots are labeled as Z and X so as to be consistent with the numerical simulation results obtained from ADAMS/View. It can be seen that the experimental results are close to the simulation results and both the experiments and simulation results show that the path deviation is less when the two DOF D4bar suspension is used. Figure 13(b) shows the error between the desired and achieved path from the experiments with and without suspension. The maximum path deviation from the desired straight line path is about 21.02 mm and 55.7 mm with and without suspension in the experiment, respectively. The path deviation between simulated and desired path is same as shown earlier in section 3. It is clear that the WMR with the D4Bar suspension deviates less from the desired straight line path and hence, we can conclude that the slip is less when the wheels are allowed lateral tilt.

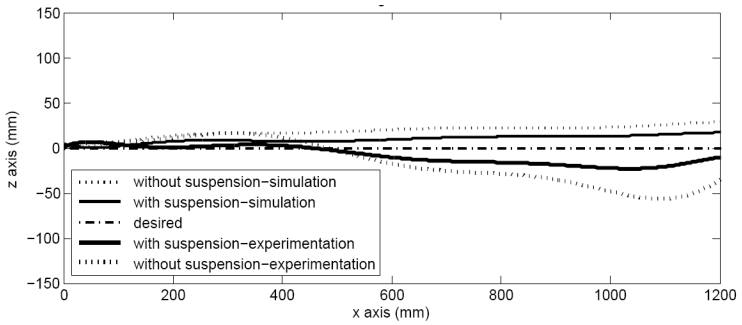

(a) Straight line path (with and without suspension): Simulation and experiments

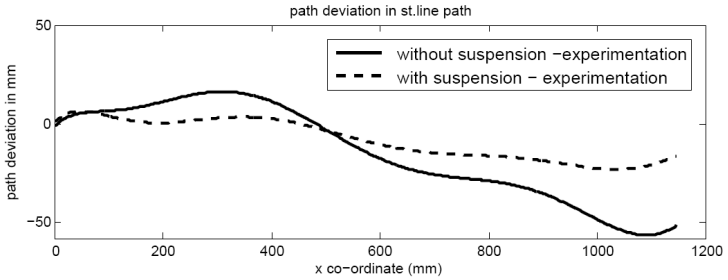

(b) Error between desired and achieved straight line path (with and without suspension)

Figure 13: Plots of straight line path with and without suspension (simulation and experiment)

Circular motion

To follow a circular path, constant steering input to front wheel is given. The experiment were carried out twice – with lateral tilting enabled and without tilting. The photograph in figure 14

shows the path traced by the marker attached to the platform centre when the WMR moves on the uneven terrain with and without lateral tilting. The plot of the path of the platform centre from simulations, experiments and the desired circular path are shown in figure 15. The path deviation error is measured and although the maximum deviation is more than 150 mm, the average value is about 39 mm with lateral tilting and 52 mm without lateral tilting. The smaller difference in path error, with and without suspension case, is due to the continuous steering which does not let the error grow as in the straight line motion.

Figure 14: Circular path with and without suspension

A lane change motion

For the lane change maneuver, the steering in the front wheel is not constant. The pattern of the steering input is chosen as $(0°) - (+30°) - (-30°) - (0°)$ with a wait time of 5 sec in between the inputs. The photograph in figure 16 shows the path traced by the marker at the platform centre on the uneven terrain. The red trace is when the suspension is not used and wheel lateral tilting is not allowed. The blue trace is with suspension and lateral tilting. Figure 17 shows the plots of the path when the WMR undergoes a lane change motion. It shows the results obtained from numerical simulation, the desired path and the path obtained from experiments. The maximum path deviation error in experiments is measured to be about 27 mm and 47.5 mm with and without

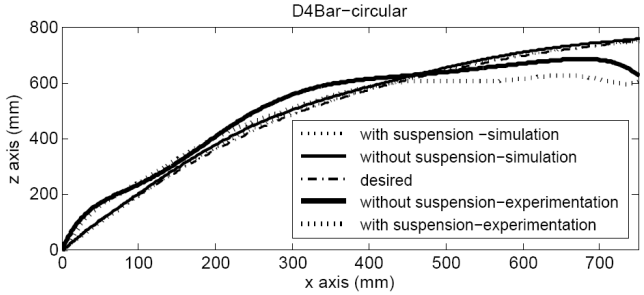

(a) Circular path (with and without suspension): Simulation and experiments

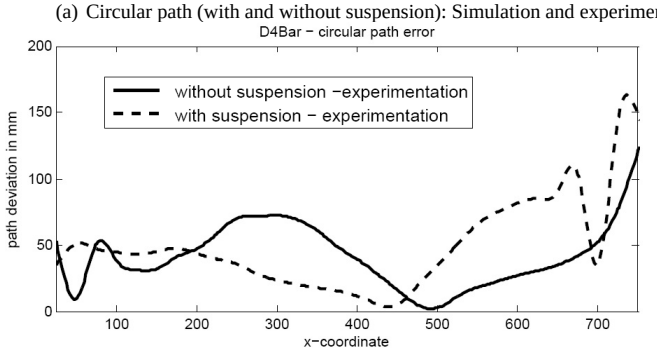

(b) Error between desired and achieved circular path (with and without suspension)

Figure 15: Plots of circular path with and without suspension (simulation and experiment)

suspension, respectively. It can be clearly seen that the path deviation is less when the two DOF D4Bar suspension, allowing lateral wheel tilt, is used.

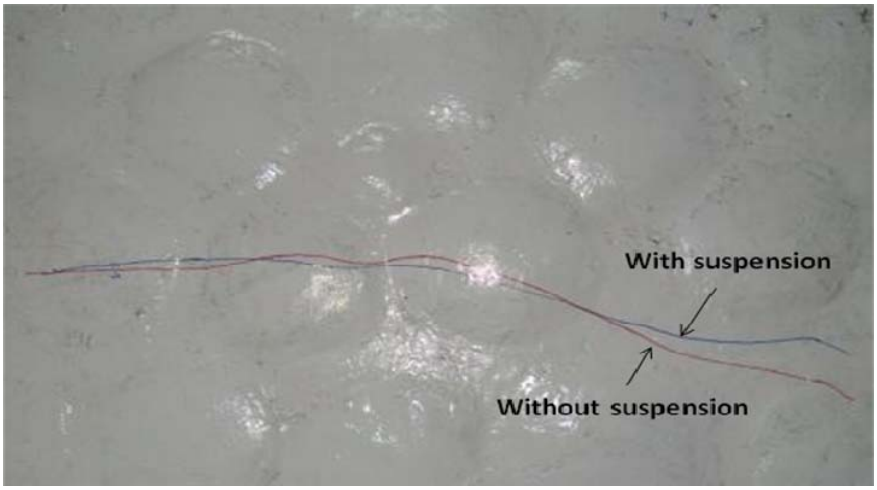

Figure 16: Lane change motion with and without suspension

From the simulation and experimental results for the three representative motions, we can

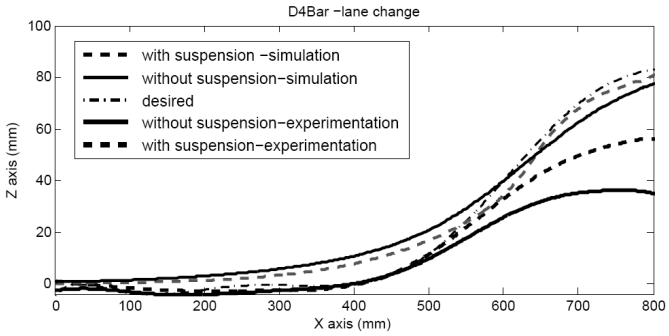

(a) Lane change path (with and without suspension): Simulation and experiments

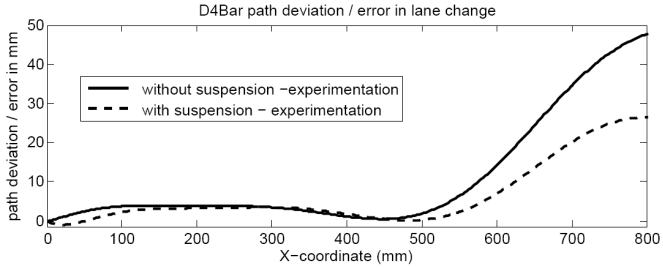

(b) Error between desired and achieved lane change path (with and without suspension)

Figure 17: Plots of lane change path with and without suspension (simulation and experiment)

clearly infer that the three-wheeled WMR can navigate better on uneven terrain when the two DOF D4Bar suspension is used. The path deviation is less when lateral tilt of the wheels are allowed and indirectly we can infer that wheel slip is significantly reduced with the lateral tilting of the torus-shaped wheels.

5 Conclusion

A novel D4Bar suspension for a WMR to traverse an uneven terrain with low slip is presented in this paper. Numerical simulations, done using ADAMS /View, show that the mobile robot will exhibit less slip when the D4Bar suspension is used while it slips much more when the suspensions is not used on uneven terrains. Experimentation was done for three motions, namely a straight line motion, a circular motion and a lane change motion. The path of the platform centre in the representative paths are projected on surface. The plot of error as function of path is presented for all the cases. Experiments clearly show that the deviation from desired trajectories and path

deviation error are much less when the D4Bar suspension is used and the torus shaped wheels are allowed to tilt laterally. Based on simulation and experimentation, which ensures both reductions in slip and less path deviation, we can conclude the D4Bar suspension will lead to less slip on uneven terrains. Future work will focus on the development of a more refined three-wheeled mobile robot and more extensive experimentation to validate the slip free capability of a wheeled mobile robot, traversing an uneven terrain, when the wheels are allowed to tilt laterally.

References

[1] Waldron, K. J., 1995, "Terrain Adaptive Vehicle", *ASME Trans., Journal of Mechanical Design*, Vol. 117B, pp. 107-112.

[2] Choi, B. J., Srinivasan S. V., and Davis P. W., 1999, "Two wheels connected by an un-actuated variable length axle on uneven ground: Kinematic modeling and experiments", *ASME Trans., Journal of Mechanical Design*, Vol. 121, pp. 235-240.

[3] Chakraborty, N. and Ghosal, A., 2004, "Kinematics of wheeled mobile robots on uneven terrain", *Mechanism and Machine Theory*, Vol. 39, pp. 1273-1287.

[4] Chakraborty, N. and Ghosal, A., 2005, "Dynamic modeling and simulation of wheeled mobile robot for traversing uneven terrain without slip", *ASME Trans., Journal of Mechanical Design*, Vol. 127, pp. 901-909.

[5] Auchter, J, Moore, C. A. and Ghosal, A., 2009, "A novel kinematic model for rough terrain robots", *Advances in Computational Algorithms and Data Analysis Lecture Notes in Electrical Engineering*, Vol. 14, pp. 215-234.

[6] Rollins, E., Luntz, J., Foessel, A., Shamah, B., and Whittaker, W., 1998, "Nomad: A demonstration of transforming chasis", *Proc. 1998 IEEE International Conference On Robotics and Automation*, Belgium, pp. 611-617.

[7] Lindamannon, R. A., Bickler, D. B., Harrington, B. D., Ortiz, G.M., and Voothees, C. J., 2006, "Mars exploration rover mobility development", *Proc. IEEE Robotics and Automation Magazine*, pp. 19-26.

[8] Kuroda, Y., Konda, K., Nakamura, K., Kunii, Y., and Kubota, T., 1999, "Low power mobility system for micro planetary rover Micro5", *Proc of i-SAIRAS 99, STEC*, The Netherlands, pp. 77-82.

[9] Siegwart, R., Lamon, P,. Estier, T., Lauria, M., and Piguet, R., 2002, "Innovative design for wheeled locomotion in rough terrains", *Journal of Robotics and Autonomous Systems*, Vol. 40, pp. 151-162.

[10] Hoshino, H., Ishikawa, A., Fukuda, T., and Hasegawa, Y., 2004, "Mobile mechanism suitable for rough terrain vehicles", *JSME International Journal*, Vol. 47, No. 2, pp. 646-652.

[11] Sreenivasan, S. V., Dutta, P. K. and Waldron, K. J., 1994, " The wheeled actively articulated vehicle (WAAV): an advanced off-road mobility concept", *Proc. of 4rth Int. Workshop on Advances in Robot Kinematics*, Ljubljana, Slovenia, 1994.

[12] Brady, R. N., 1989, *Heavy-Duty Truck Suspension, Steering, and Braking Systems*, Prentice Hall Publications, New Jersey, USA.

[13] Dixon, J. C., 1996, *Tires, Suspension and Handling, Second Edition*, Society of Automotive Engineers, Arnold, London.

[14] Sebe, M., 2003, US Patent 6511078 B2, " Vehicle having suspension system with variable camber and vertical suspension in the plane of the wheel".

[15] Krajekian, G., 2014, US Patent 8641064 B2, "Tilting vehicle with non-tilting automobile like body".

[16] Weiss, W., 2001, US Patent 6,267,387, "Wheel suspension with automatic camber adjustment".

[17] Laurent, D., 2002, US Patent 6,406,036, "Vehicle suspension having active camber variation".

[18] Choudhery, K. M., 2005, US Patent 6,874,793, "Variable camber suspension system".

[19] Tharakeshwar Appala, 2012, *Novel suspension mechanism for three wheeled mobile robot traversing uneven terrain without slip*, Ph.D Thesis, Indian Institute of Science, Bangalore, India.

[20] Tharakeshwar Appala and Ghosal, A., 2013, "A three-wheeled mobile robot for traversing uneven terrain without slip: Simulation and experiments", *Mechanics based Design of Structures and Machines*, Vol. 41, pp. 60-78.

[21] Montana, D. J., 1988, "The kinematics of contact and grasp", *Int. Journal of Robotics Research*, Vol. 7, No. 3, pp. 17-32.

[22] *MATLAB, Version 7.10 R(2010a)*, 2010, The MathWorks Inc., Natick, Masschusetts, USA

[23] *MSC Software ADAMS/View*, 2013, MSC Software Corporation, Newport Beach, California, USA.

[24] Robert Bosch GmbH, 2007, *Automotive Handbook, 7th Edition*, Bentley Publication, Cambridge, MA, USA.

[25] *SolidWorks 3D CAD*, 2013, Dassault Systémes SolidWorks Corp., Waltham, MA, USA.

[26] *LEGO Mindstrom NXT 2.0*, 2009, LEGO Systems, Inc., Enfield, CT, USA.

List of Figure Captions

Figure 1: Torus-shaped wheel on uneven terrain

Figure 2: A three-wheeled mobile robot with torus-shaped wheels on uneven terrain

Figure 3: The two DOF D4Bar suspension

Figure 4: Numerical simulation of straight line motion

Figure 5: Wheel slip in circular motion

Figure 6: Simulation of circular motion and error from desired path

Figure 7: Simulation of a lane change motion

Figure 8: Exploded view of one wheel, suspension components and WMR platform

Figure 9: Schematic of arrangement for transmission of power

Figure 10: Prototype three-wheeled WMR

Figure 11: Snapshots of straight line motion of the WMR

Figure 12: Straight line path with and without suspension

Figure 13: Plots of straight line path with and without suspension (simulation and experiment)

Figure 14: Circular path with and without suspension

Figure 15: Plots of circular path with and without suspension (simulation and experiment)

Figure 16: Lane change motion with and without suspension

Figure 17: Plots of lane change path with and without suspension (simulation and experiment)

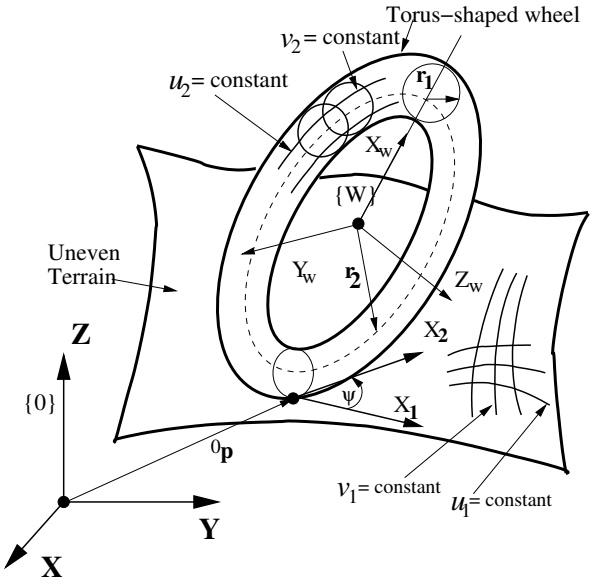

Figure 1: Torus-shaped wheel on uneven terrain

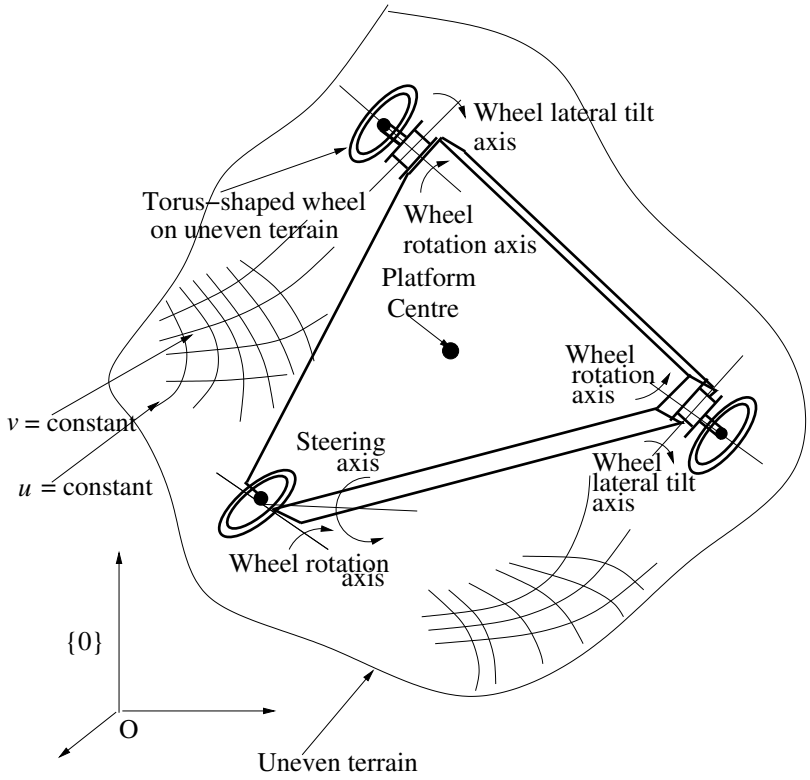

Figure 2: A three-wheeled mobile robot with torus-shaped wheels on uneven terrain

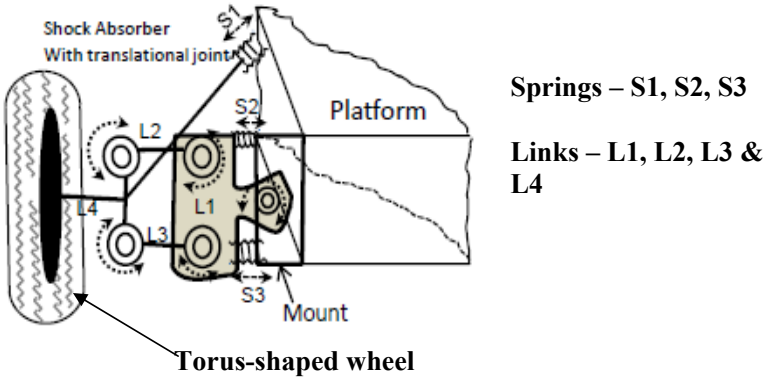

Figure 3: The two DOF D4Bar suspension

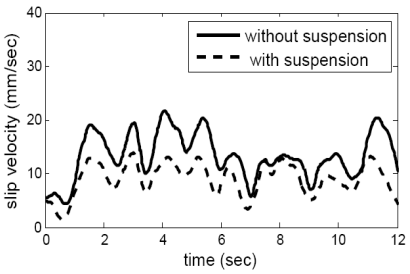

(a) Slip velocity at left wheel

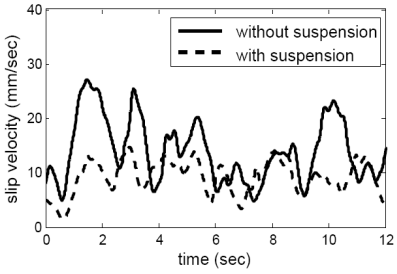

(b) Slip velocity at right wheel

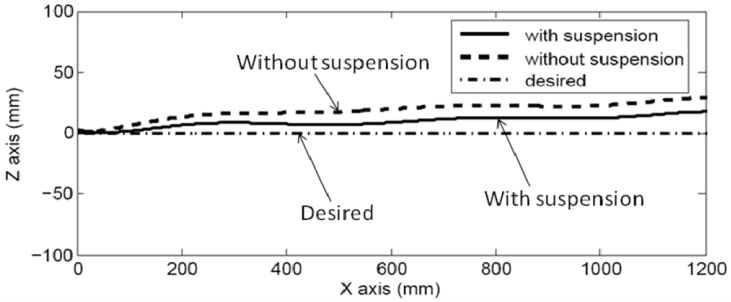

(c) Straight line path with and without suspension

Figure 4: Numerical simulation of straight line motion

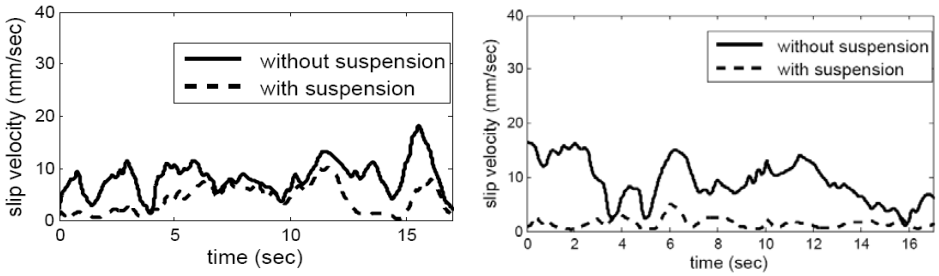

(a) Left wheel slip velocity (b) Right wheel slip velocity

Figure 5: Wheel slip in circular motion

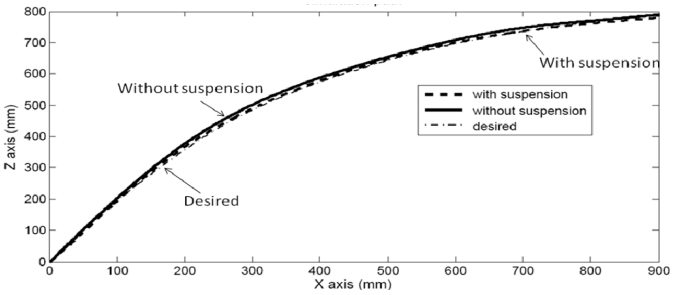

(a) Circular path with and without suspension

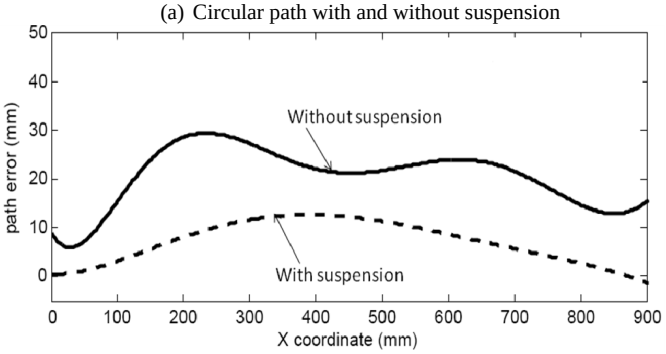

(b) Error between desired and simulated path

Figure 6: Simulation of circular motion and error from desired path

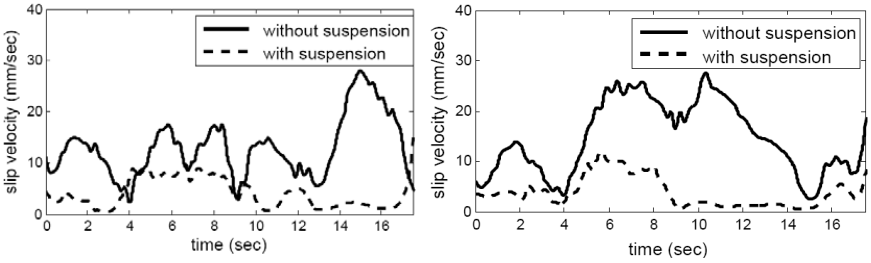

(a) Left wheel slip velocity

(b) Right wheel slip velocity

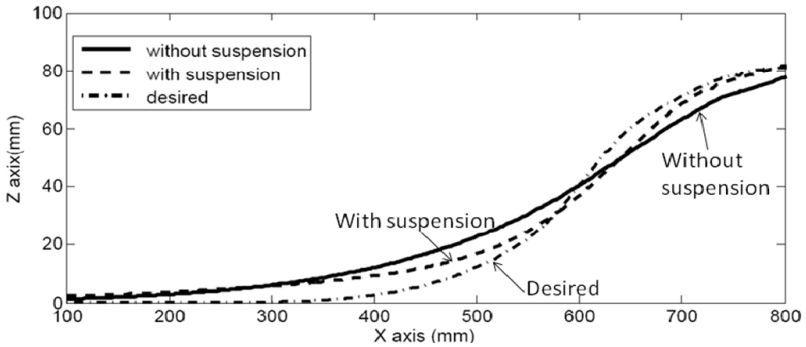

(c) Lane change path with and without suspension

Figure 7: Simulation of a lane change motion

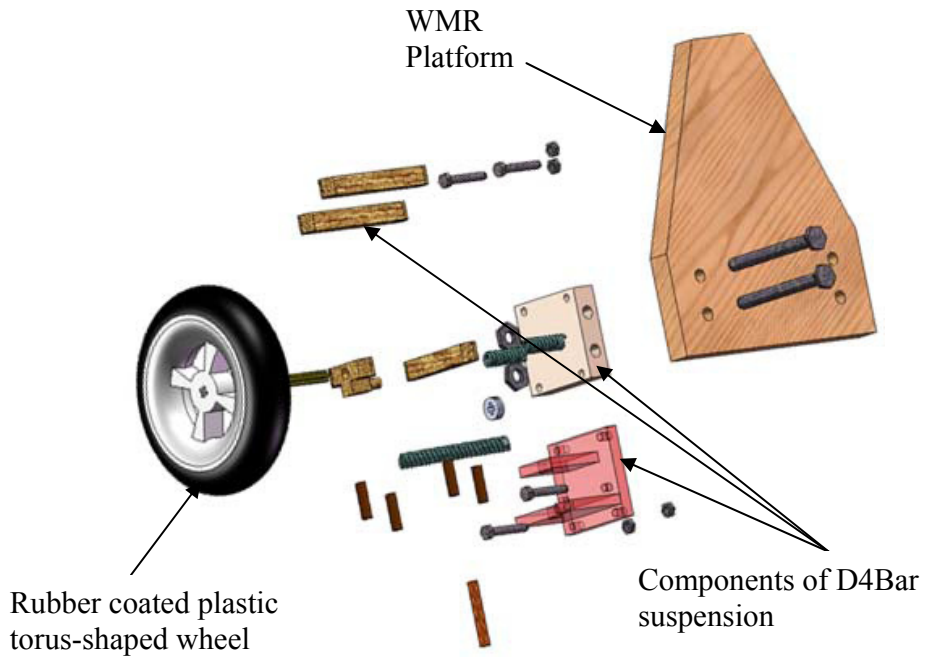

Figure 8: Exploded view of one wheel, suspension components and WMR platform

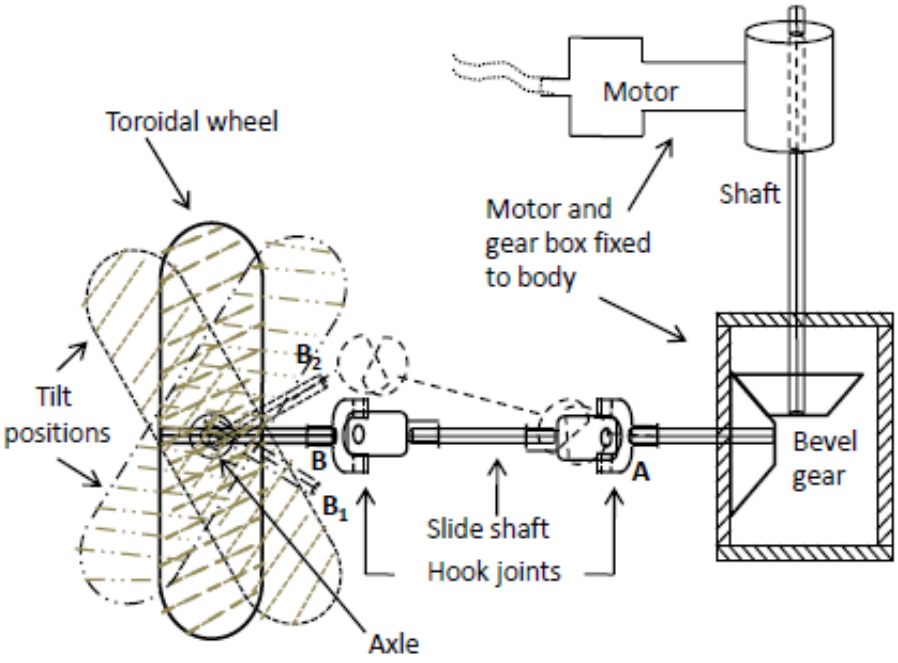

Figure 9: Schematic of arrangement for transmission of power

Figure 10: Prototype three-wheeled WMR

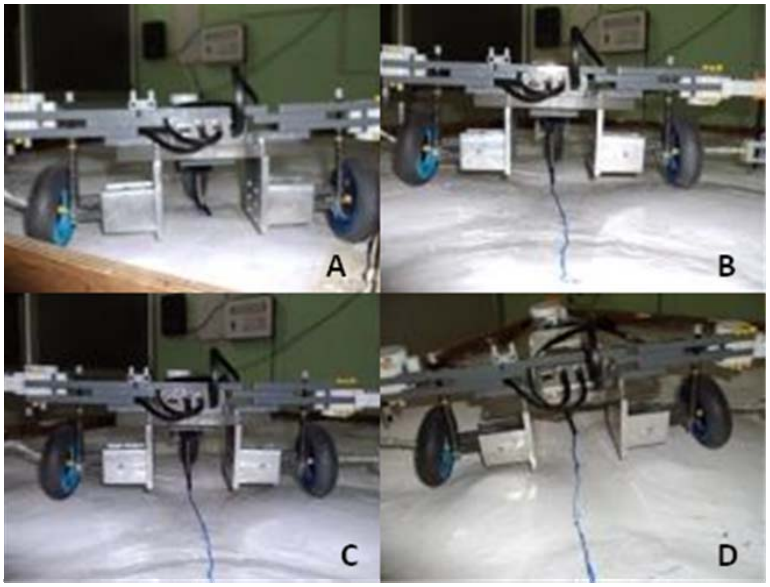

Figure 11: Snapshots of straight line motion of the WMR

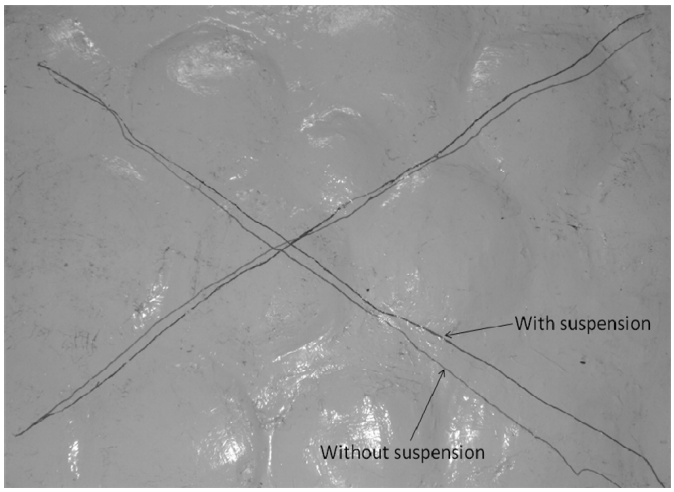

Figure 12: Straight line path with and without suspension

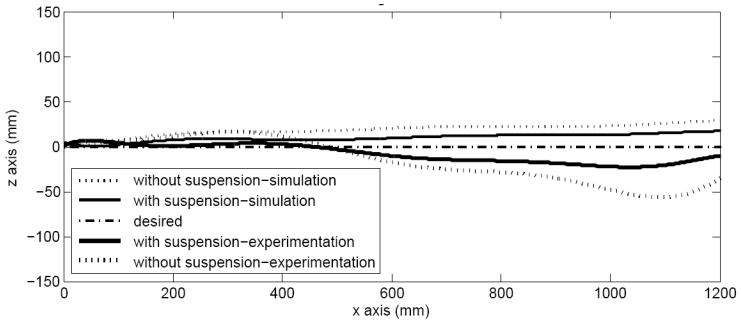

(a) Straight line path (with and without suspension): Simulation and experiments

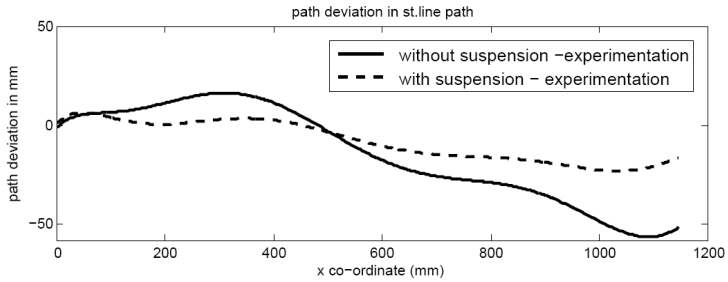

(b) Error between desired and achieved straight line path (with and without suspension)

Figure 13: Plots of straight line path with and without suspension (simulation and experiment)

Figure 14: Circular path with and without suspension

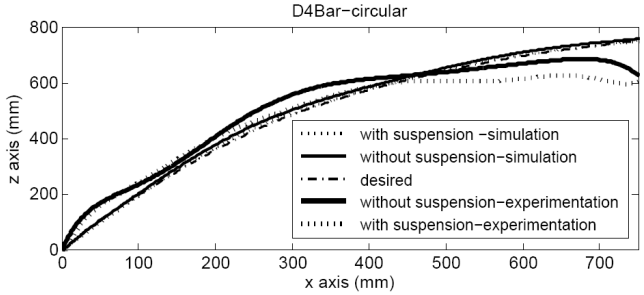

(a) Circular path (with and without suspension): Simulation and experiments

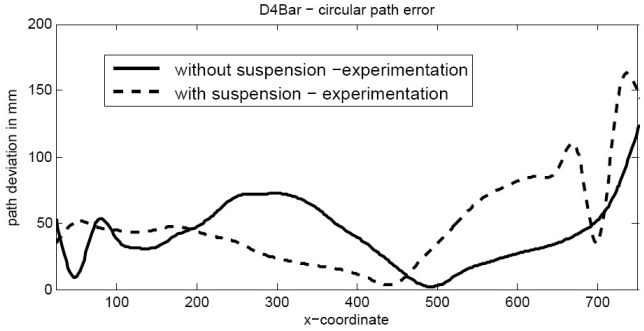

(b) Error between desired and achieved circular path (with and without suspension)

Figure 15: Plots of circular path with and without suspension (simulation and experiment)

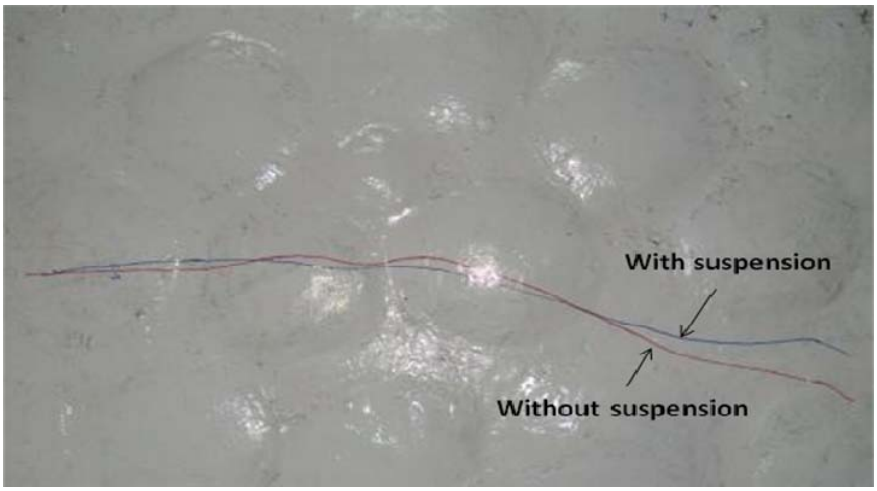

Figure 16: Lane change motion with and without suspension

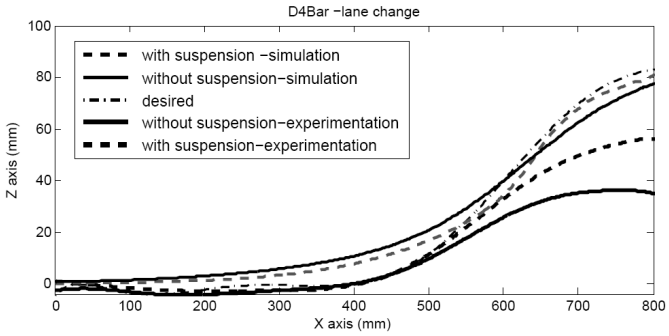

(a) Lane change path (with and without suspension): Simulation and experiments

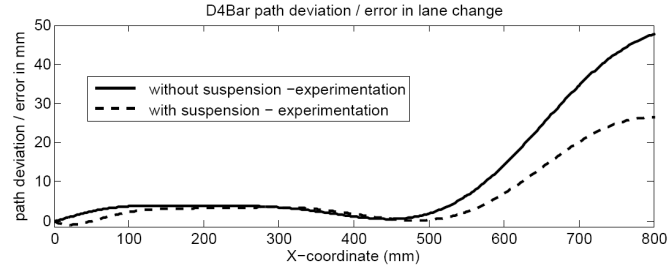

(b) Error between desired and achieved lane change path (with and without suspension)

Figure 17: Plots of lane change path with and without suspension (simulation and experiment)